

# Innovative Catalytic Strategies: The Game - Changing Role of S - Doping in NiFe Layered Double Hydroxides (LDHs) for Superior Water Oxidation

Manoj Kumar<sup>1</sup>, Raghvendra Pratap Singh<sup>2</sup>

<sup>1</sup>Department of Chemistry, Kamla Nehru Institute of Physical and Social Sciences, Sultanpur UP - 228118, India  
Email: [manojkumar35036\[at\]gmail.com](mailto:manojkumar35036[at]gmail.com)

<sup>2</sup>Department of Chemistry, Kamla Nehru Institute of Physical and Social Sciences, Sultanpur UP - 228118, India  
Corresponding Author Email: [rpsinghkni\[at\]gmail.com](mailto:rpsinghkni[at]gmail.com)

**Abstract:** *In the quest for sustainable energy solutions, the efficient production of oxygen and hydrogen through water oxidation has emerged as a critical area of research. The electrochemical water splitting can fulfill the future global energy demand by producing clean and eco-friendly H<sub>2</sub>. As the anodic oxygen evolution reaction (OER) of water splitting is kinetically sluggish and accompanied by the input of extra overpotential, a low cost and highly efficient electrocatalyst must be developed for efficient OER activity. Herein, we have explored a room temperature method for the S - doping in NiFeOOH nanosheets for the excellent OER activity. The S - doping in NiFeOOH modulated the electronic structure, increases the number of active sites and improved electrochemical surface area enhancing the OER activity. The S - NiFeOOH showed excellent OER activity and required only 200 mV overpotential to produce 50 mA cm<sup>-2</sup> current density in comparison to un - doped NiFeOOH. Moreover, S - NiFeOOH exhibited 24 h chronoamperometric (CA) stability for the O<sub>2</sub> production at high current density.*

**Keywords:** S - doping; ultrathin S - NiFeOOH nanosheets; electronic structure modulation; water splitting; oxygen evolution

## Highlights

- Facile synthesis of NiFeOOH nanosheets at room temperature.
- Doping of S in NiFeOOH nanosheets.
- Modulation of the electronic structure of NiFeOOH by S - doping.
- Excellent oxygen evolution activity by S - NiFeOOH nanosheets.

## 1. Introduction

The increasing global energy demand and environmental problems can be solved by introducing electrochemical water splitting as a sustainable energy conversion technology<sup>1, 2</sup>. The electrochemical water splitting leads to the formation of H<sub>2</sub> and O<sub>2</sub> by two half - cell reactions i. e. hydrogen evolution reaction (HER) at cathode and oxygen evolution reaction (OER) at anode, respectively<sup>3-5</sup>. Generally, anodic OER is a thermodynamically uphill reaction (input of 1.23 V vs RHE) and follows sluggish kinetics due to the four electron and proton transfer mechanism<sup>6-9</sup>. In addition, a number of high energy intermediates are generated during the reaction<sup>10-14</sup>. As a result, extra energy in form of overpotential is demanded to overcome the sluggish kinetics and proceed the overall water oxidation reaction.

In this regard, noble metal based RuO<sub>2</sub>, IrO<sub>2</sub> catalysts have been well studied for electrochemical OER with good catalytic activity<sup>15-20</sup>. However, their large - scale practical application is inhibited due to their high price and rare earth abundance. Therefore, it is very challenging to develop an efficient, cost effective, and stable OER electrocatalysts from

earth abundant transition metals. In recent years, first row transition metal (Ni, Co, Fe, Mn) based catalysts such as oxides, chalcogenides, phosphides, carbide and nitrides have been explored for electrochemical OER due to their enhanced catalytic activity and stability<sup>21-26</sup>.

Recently, the studies have shown that transition metal - based oxides, chalcogenides, phosphides and nitrides act as precatalysts and undergo electrochemical reconstruction into metal - (oxy) hydroxide [M (O) OH] active catalysts under applied anodic potential in alkaline medium<sup>4, 13, 21, 27-30</sup>. For example, Indra et al. developed the cobalt phosphonate (CoP<sub>n</sub>) on nickel foam and employed for the OER<sup>31</sup>. The CoP<sub>n</sub> was electrochemically transformed into layered Co (O) OH under applied anodic potential, which was the real active catalyst for OER<sup>31</sup>. The formation of active Co (O) OH was established by *in - situ* X - ray absorption spectroscopy<sup>14, 32, 33</sup>. The CoP<sub>n</sub> achieved 10 mAcm<sup>-2</sup> current density at an overpotential of 240 mV for OER<sup>31</sup>. Similarly, Hu et al. prepared NiFeP electrocatalyst for electrochemical OER. Interestingly, NiFeP was also converted into active NiFeOOH catalyst under applied anodic potential during OER. The catalyst showed superior OER activity at an overpotential of 219 mV to attain 10 mA cm<sup>-2</sup> current density<sup>5, 16, 34-38</sup>. The active M (O) OH catalyst possesses high surface area, more exposed active sites, good electronic conductivity and improved charge and mass transfer to improve the OER activity<sup>6, 11, 35, 39</sup>.

In this regard, several NiFe - based electrocatalysts such as NiOOH, FeOOH, NiFeOOH and so on have been explored for the excellent electrochemical OER activity<sup>40-43</sup>. For

Volume 13 Issue 10, October 2024

Fully Refereed | Open Access | Double Blind Peer Reviewed Journal

[www.ijsr.net](http://www.ijsr.net)

example, Hu et al. synthesized mixed phase FeOOH electrocatalyst by hydrothermal method for electrochemical OER. The mixed phase FeOOH showed excellent OER activity in alkaline medium and attained  $10 \text{ mA cm}^{-2}$  current density only at an overpotential of 180 mV<sup>41</sup>. Further, Zhang et al. also reported Ni/FeOOH for OER at low overpotential of 290 mV to achieve  $50 \text{ mA cm}^{-2}$  current density. The Ni/FeOOH showed improved OER activity due to improved efficiency of charge transfer and mass diffusion to active centers<sup>44</sup>. Similarly, Ma et al. prepared FeOOH nanosheets on Ni - Foam for the enhanced OER activity in alkaline medium. The synthesized catalyst attained  $10 \text{ mA cm}^{-2}$  current density only at an overpotential of 235 mV<sup>45</sup>.

Although several NiFe - based (oxy) hydroxide catalysts have been reported for the electrochemical OER, their OER activity is not up to the practical mark. Several strategies have been employed to tune the electronic structure of metal - (oxy) hydroxide active catalyst in which the heteroatom doping is considered as an effective way to tune the structural and electronic properties of (oxy) hydroxide improving the OER activity<sup>46-48</sup>. For example, Guo et al. prepared sulphur doped FeOOH (S - FeOOH) by hydrothermal method and utilized for the electrochemical OER. The S - doping was observed to improve the OER activity as the required overpotential for FeOOH was decreased from 294 mV to 254 mV after S - doping to reach  $50 \text{ mA cm}^{-2}$  current density<sup>49</sup>. The S - doping optimized the binding energy for the adsorption of the reaction intermediates to promote the OER activity<sup>49,50</sup>.

In another report, Li et al. synthesized nitrogen doped NiFeOOH (N - NiFeOOH) catalyst for the electrochemical OER. The N - NiFeOOH showed 243 mV overpotential for  $10 \text{ mA cm}^{-2}$  current density, lower than that of NiFeOOH (287 mV)<sup>48</sup>. The DFT results showed that the N - doping

lowered the d - band centers promoting the adsorption of oxygen intermediates<sup>48</sup>. The studies have revealed that the doping of heteroatoms in electrocatalyst improves the distribution of active sites, increases the electrochemically active surface area and improves the oxygen diffusion in active sites [51 - 53]. As a result, enhanced OER activity was recorded at low overpotentials.

Inspired by the previous studies, an attempt has been made to develop cheap and cost - efficient NiFe - based active catalyst for the improved OER activity in alkaline medium. We have prepared nickel iron - (oxy) hydroxide (NiFeOOH) catalyst on nickel foam (NF) using solvothermal method at room temperature. Further, sulphur doping has been performed to develop S - NiFeOOH catalyst using similar conditions to investigate the effect of S - doping in NiFeOOH (Figure 1). Generally, NiFeOOH catalyst was prepared by the hydrothermal method and the doping of heteroatoms was also carried out hydrothermally at high temperature and pressure<sup>49</sup>. In contrast, we have demonstrated S - NiFeOOH at room temperature by galvanic deposition method (Figure 1, see experimental section).

Interestingly, S - NiFeOOH required only 200 mV overpotential to afford  $50 \text{ mA cm}^{-2}$  current density, lower than that of un - doped NiFeOOH (240 mV). The S - doping resulted in the lower Tafel slope indicating the faster OER kinetics for S - NiFeOOH compared to the NiFeOOH. Moreover, S - NiFeOOH showed chronoamperometric (CA) stability for 24 h at high current density without no significant loss in initial current. The improved OER activity, kinetics and stability were attributed to the modulated electronic properties of NiFeOOH due to S - doping. The S - doping optimized the binding energy for the reaction intermediates promoting the facile O - O bond formation.

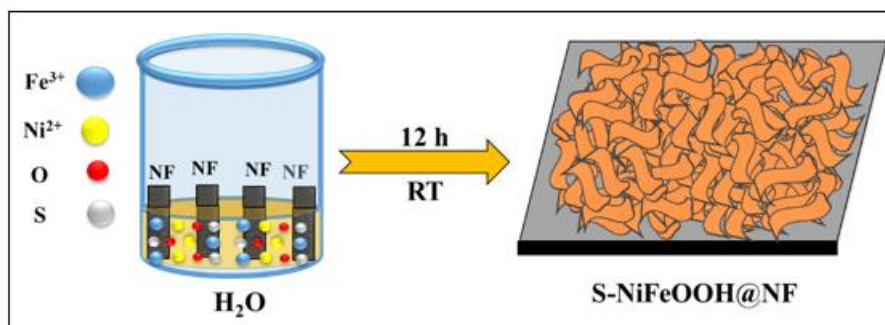


**Figure 1:** Schematic illustration for the designing of S - NiFeOOH on nickel foam using simple solvothermal method at room temperature.

## 2. Experimental Section

### 2.1 Activation of Nickel Foam (NF)

Nickel foam (NF) was cut into small pieces with the dimensions of  $1 \text{ cm} \times 2 \text{ cm}$ . The pieces of NF were sonicated into 1.0 M HCl solution under ultra - sonication for 15 minutes to eliminate the oxide layer and impurities from the surface of NF. Afterwards, NF films were washed with double distilled water several times. Further, the NF films were dried in an air oven for overnight and used for the preparation of the catalyst films.

### 2.2 Synthesis of NiFeOOH (NiFeOOH)

For the synthesis of NiFeOOH, 60 mmol of  $\text{Fe}(\text{NO}_3)_3 \cdot 9\text{H}_2\text{O}$  was dissolved into 5 ml of water in a glass vial to make homogeneous solution. A piece of NF was dipped vertically inside the solution and kept for 12 hours at room temperature. Afterwards, the film was removed from the solution and washed three times with double distilled water. As synthesized NiFeOOH films was dried at  $60^\circ \text{C}$  in an air oven overnight.

### 2.3 Synthesis of sulphur doped NiFeOOH (S - NiFeOOH)

For the preparation of S - NiFeOOH, a homogeneous solution was prepared by dissolving 60 mmol of  $\text{Fe}(\text{NO}_3)_3 \cdot 9\text{H}_2\text{O}$  in 5 ml of  $\text{H}_2\text{O}$  in a glass vial. Further, 20 mg of  $\text{Na}_2\text{S}_2\text{O}_3$  was added into the solution and stirred for 10 minutes. After that, a fresh film of NF was dipped vertically inside the solution and kept for 12 hours at room temperature. The film was removed from the vial and washed with double distilled water for several times. As synthesized S - NiFeOOH film was dried for 12 hours in an air oven.

Similarly, the amount of  $\text{Na}_2\text{S}_2\text{O}_3$  was also varied to synthesize different S - NiFeOOH catalysts for the comparison purpose. The S - NiFeOOH - 10 was prepared by taking 10 mg of  $\text{Na}_2\text{S}_2\text{O}_3$  while S - NiFeOOH - 30 was synthesized using 30 mg of  $\text{Na}_2\text{S}_2\text{O}_3$ .

### 3. Understanding S - Doping: What It Is and How It Works

S - doping, or sulfur doping, is a fascinating modification technique that significantly enhances the catalytic properties of materials, particularly in the realm of layered double hydroxides (LDHs) like NiFe LDHs. At its core, S - doping involves the intentional introduction of sulfur atoms into the material's crystal lattice, which alters its electronic structure and surface chemistry. This process can create new active sites for catalytic reactions, effectively boosting the material's reactivity and efficiency.

The mechanism behind S - doping is rooted in the unique properties of sulfur. By substituting oxygen atoms with sulfur in the hydroxide layers of NiFe LDHs, the electronic configuration of the material is modified. This alteration can lead to a reduction in the bandgap energy, facilitating easier electron transfer during the water oxidation process. As a result, the doped material exhibits enhanced oxygen evolution reaction (OER) activity, which is crucial for applications in water splitting and renewable energy production.

Moreover, S - doping can improve the stability and durability of NiFe LDHs under operational conditions. The incorporation of sulfur can help mitigate the leaching of metal ions, ensuring that the catalysts retain their integrity over time. This aspect is particularly critical in practical applications where longevity and consistent performance are desired.

By understanding the principles of S - doping and its implications for the catalytic performance of NiFe layered double hydroxides, researchers can design more effective catalysts for water oxidation. This innovative approach not only unlocks the potential of existing materials but also paves the way for the development of new, high - performance catalysts that contribute to sustainable energy solutions. As the quest for efficient and eco - friendly water splitting technologies continues, S - doping stands out as a promising strategy in the field of catalysis.

### 4. Mechanisms of Enhanced Activity through S - Doping

The enhanced catalytic activity observed in S - doped NiFe layered double hydroxides (LDHs) can be attributed to a

combination of electronic, structural, and thermodynamic factors that work synergistically to optimize the water oxidation process<sup>24, 46, 52, 53</sup>. At the core of this enhancement lies the introduction of sulfur (S) into the LDH structure, which modifies the electronic properties of the catalyst and creates new active sites that facilitate the oxidation of water.

One of the primary mechanisms driving enhanced activity is the alteration of the electronic band structure due to S - doping. Sulfur atoms can introduce additional electronic states within the band gap of the NiFe LDHs, effectively lowering the energy barrier for charge transfer processes. This results in increased conductivity and improved electron mobility, allowing for more efficient electron - hole pair generation during the catalytic cycle. As a consequence, the kinetics of the water oxidation reaction are significantly accelerated, leading to higher overall reaction rates.

Furthermore, S - doping impacts the surface morphology and stability of the NiFe LDHs. The incorporation of sulfur can lead to a more favorable arrangement of metal ions, enhancing the structural integrity of the catalyst under operational conditions. This stability is crucial as it ensures sustained catalytic performance over extended periods, minimizing deactivation and loss of activity.

Additionally, the presence of sulfur can modify the local coordination environment of the metal centers, which plays a vital role in the activation of water molecules. The unique bonding characteristics of sulfur may enhance the adsorption energy of water on the catalyst surface, promoting the formation of reactive hydroxyl species that are essential for efficient oxidation. This not only elevates the reaction rate but also improves the catalyst's selectivity towards desired products.

### 5. Electrochemical measurements

A single - compartment three - electrode electrochemical cell was used for the electrochemical measurement in 1.0 M aqueous KOH electrolyte (pH 13.8). The synthesized catalysts@NF were utilized as the working electrode, Pt wire as counter electrode and Ag/AgCl as reference electrode. The 70% iR compensation have been performed during cyclic voltammetry (CV) and linear sweep voltammetry (LSV). All the potential measurements were expressed against reversible hydrogen electrode (RHE). The equation used for potential measurement was as -

$$E(\text{RHE}) = E(\text{Ag/AgCl}) + 0.197 + 0.059\text{pH}$$

Electrochemical impedance spectroscopic (EIS) measurements have been recorded between the frequency range 0.001 to 100, 000 Hz with the amplitude of 10 mV. In Nyquist plot, semicircle's diameter was utilized to measure the charge transfer resistance ( $R_{ct}$ ). The chronoamperometric measurement (CA) was carried out under a fixed applied potential and presented without iR compensation. Tafel plots were determined by potentiostatic measurements at that potential where current density reached up to  $10 \text{ mA cm}^{-2}$ . The double - layer capacitance ( $C_{dl}$ ) was determined to evaluate the electrochemically active surface areas (ECSAs).

The CV experiment was performed to measure  $C_{dl}$  at that potential range where faradaic process was not observed.

## 6. Result and discussion

The formation of NiFeOOH was first confirmed using the powder X-ray diffraction (PXRD) technique. The PXRD pattern was indexed for the mixed phase of  $\alpha$ -Ni(OH)<sub>2</sub> (JCPDS No - 38 - 0175) and  $\beta$ -FeOOH (JCPDS No - 75 - 1594) for both NiFeOOH and S-NiFeOOH (Figure 2)<sup>54</sup>. It should be mentioned here that no extra peaks were generated after S-doping indicating the formation of pure  $\alpha$ -Ni(OH)<sub>2</sub> and  $\beta$ -FeOOH phase.

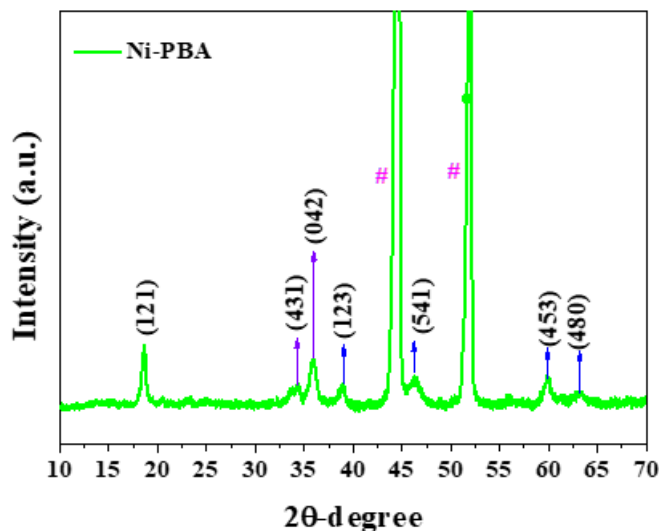


Figure 2. The PXRD pattern of Ni - PBA. The peaks were well indexed for the Ni - PBA. All the diffraction peaks were unambiguously assigned to the Hofmann - type Ni (H<sub>2</sub>O)<sub>2</sub> [Ni (CN)<sub>4</sub>]. xH<sub>2</sub>O - PBA with a 2D layered structure, which was also consistent with the reported literature. The # marked

peaks were originated from the nickel foam. The X-ray photoelectron spectroscopy (XPS) was used to investigate the electronic state of the elements in the synthesized catalysts. The Ni 2p XP spectrum of NiFeOOH was deconvoluted into two peaks at 856.02 eV and 873.45 eV, corresponded to the Ni 2p<sub>3/2</sub> and Ni 2p<sub>1/2</sub>, respectively<sup>55, 56</sup>. The peaks at 855.31 eV and 857.03 eV were corresponded to Ni<sup>2+</sup> and Ni<sup>3+</sup> species, respectively. The comparison of Ni 2p XPS of S-NiFeOOH indicated the positive shift of 1.65 eV in Ni 2p<sub>3/2</sub> peaks towards higher binding energy compared to that of NiFeOOH (Figure 3 - a)<sup>56</sup>. This result suggested the presence of more amount of high valent Ni<sup>3+</sup> species in S-NiFeOOH due to S-doping. Moreover, the shift of binding energy in Ni 2p XPS clearly demonstrated the modulation of the electronic properties of Ni due to S-doping.

The Fe 2p XPS of NiFeOOH was deconvoluted into two main peaks at 712.43 and 725.83 eV corresponded to Fe 2p<sub>3/2</sub> and Fe 2p<sub>1/2</sub>, respectively (Figure 3b)<sup>57</sup>. The peak observed at 712.18 eV was attributed to Fe<sup>3+</sup> species<sup>58</sup>. The Fe 2p XPS of S-NiFeOOH was also deconvoluted into two peaks at 712.41 eV and 724.94 eV for Fe 2p<sub>3/2</sub> and Fe 2p<sub>1/2</sub>, respectively (Figure 3c)<sup>57, 59, 60</sup>.

The two peaks were fitted for S 2p XPS spectrum of S-NiFeOOH at 163.88 eV and 161.34 eV for S 2p<sub>1/2</sub> and S 2p<sub>3/2</sub> respectively (Figure 3d)<sup>24, 61</sup>. The XPS spectra of NiFeOOH for O 1s was deconvoluted into two peaks at binding energies 529.30 eV and 531.57 eV corresponded to M-O bond and surface -OH groups, respectively<sup>61</sup>. In O 1s XPS of S-NiFeOOH, the peaks at 529.40 eV and 532.87 eV were corresponded to M-O bond and surface -OH groups, respectively. The peak for -OH group was shifted positively by 1.30 eV compared to the NiFeOOH. This positive shift also indicated the modulation of the electronic density around the O-atom due to S-doping<sup>39, 62-64</sup>.

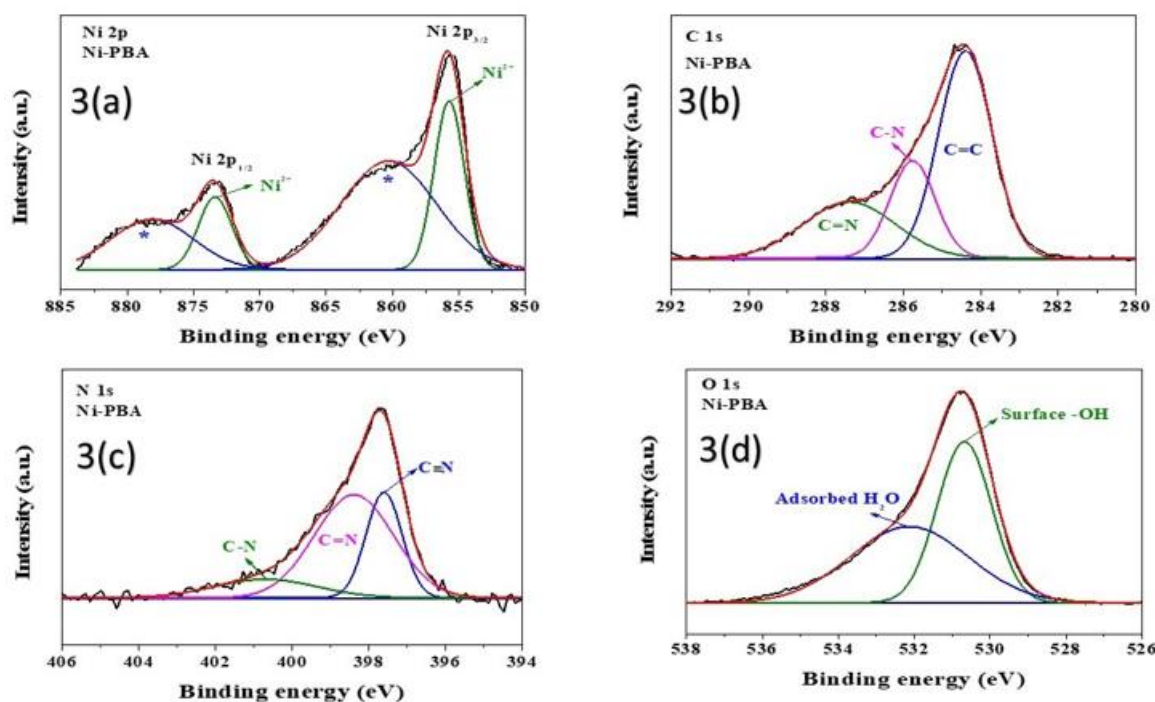


Figure 3: The X-ray photoelectron spectroscopy (XPS) of (3a) Ni 2p XPS of Ni - PBA (3b). C 1s XPS of Ni - PBA (3c) N 1s XPS of Ni - PBA (3d) O 1s XPS of Ni - PBA

## 7. Electrochemical Performance

The electrochemical properties of synthesized catalysts were measured in 1.0 M KOH solution using a single - compartment three - electrode electrochemical cell. In cyclic voltammetry (CV) profiles of NiFeOOH and S - NiFeOOH, a peak was appeared at  $\sim 1.35$  V vs RHE, which indicated the electrochemical oxidation of  $\text{Ni}^{2+}$  in to  $\text{Ni}^{3+}$  under applied anodic potential during OER (Figure S13) <sup>65</sup>.

The S - NiFeOOH showed excellent OER activity and achieved  $50 \text{ mA cm}^{-2}$  current density only at 200 mV overpotential in comparison to NiFeOOH (240 mV) (Figure 3a). Moreover, S - NiFeOOH exhibited excellent OER activity compared to S - NiFeOOH - 10 and S - NiFeOOH - 30, which produced the same current density at the overpotentials of 218 mV and 230 mV, respectively (Figure S14). These results indicated that the S - doping drastically enhanced the OER activity of NiFeOOH by reducing the overpotentials. The S - NiFeOOH exhibited superior OER activity compared to the noble metal - based  $\text{RuO}_2$  catalyst (Figure S15). Moreover, S - NiFeOOH was superior or comparable OER catalyst than the other previously reported nickel based catalysts and layered double hydroxides (LDHs).

The Tafel slope was utilized to determine the kinetics of the catalysts for the electrochemical OER. The value of Tafel slope for S - NiFeOOH was  $48 \text{ mV dec}^{-1}$ , which was very low compared to the NiFeOOH ( $98 \text{ mV dec}^{-1}$ ) (Figure 3b). The results revealed that the S - doping fasten the reaction kinetics of OER for S - NiFeOOH. The chronoamperometry was carried out to investigate the stability of S - NiFeOOH. The catalyst S - NiFeOOH showed the CA stability for 24 h under applied anodic potential without negligible loss of current density (Figure 3c). Initially, the current density was decreased for few hours due to the activation of S - NiFeOOH catalyst and further the current density was stabilized and current became constant for 24 h.

The factors related to the excellent electrochemical activity of S - NiFeOOH were further investigated. Firstly, the electrochemical impedance spectroscopy (EIS) was performed to evaluate the charge transfer properties. The smaller radius of the semicircle in EIS plot indicated the lower charge transfer resistance ( $R_{ct}$ ) of S - NiFeOOH compared to NiFeOOH. The values of  $R_{ct}$  for S - NiFeOOH and NiFeOOH were calculated to be  $0.50 \Omega$  and  $1.23 \Omega$ , respectively (Figure 3d). The lower charge transfer resistance ( $R_{ct}$ ) of S - NiFeOOH was attributed to the S - doping, which increased the electronic conductivity and charge transfer properties.

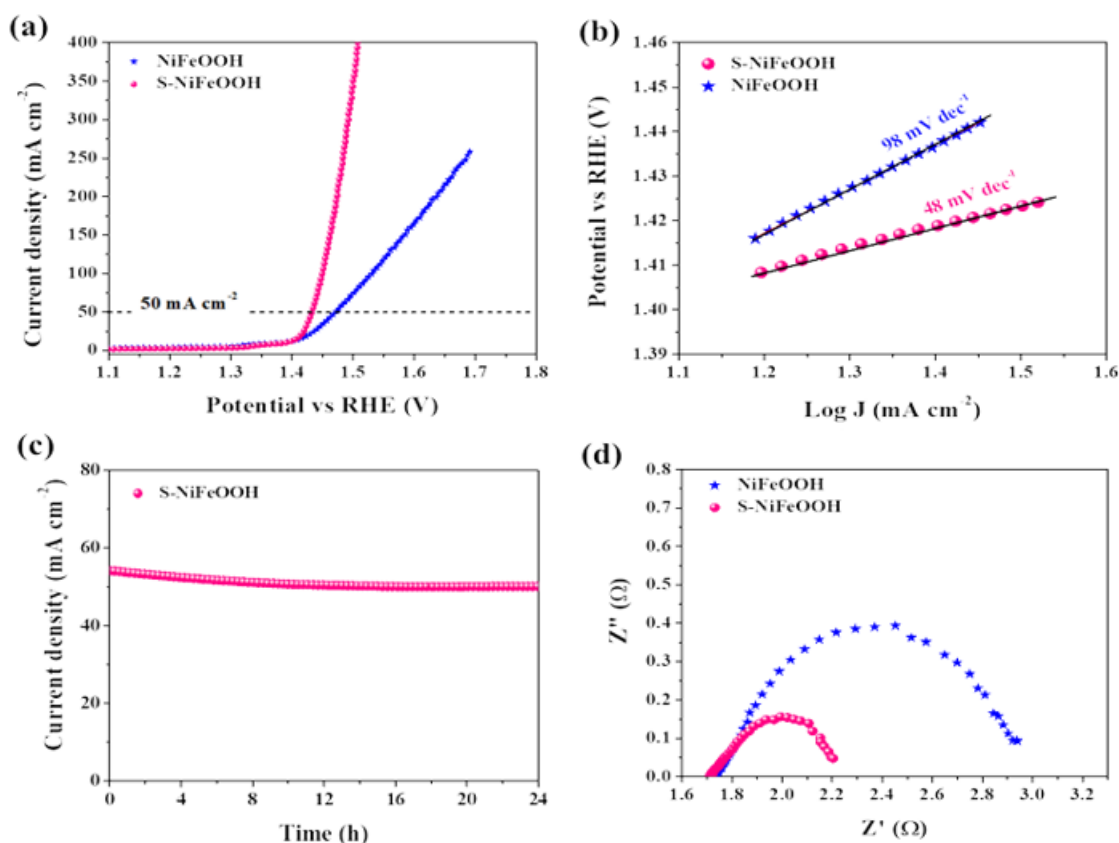


**Figure 2.** (a) LSV profiles for the oxygen evolution reaction of S - NiFeOOH and NiFeOOH showing the improved OER activity of S - NiFeOOH; (b) Tafel plots of S - NiFeOOH and NiFeOOH showing the lower Tafel slope of S - NiFeOOH; (c) EIS plots of S - NiFeOOH and NiFeOOH indicating the lower  $R_{ct}$  of S - NiFeOOH and (d) CA stability test of S - NiFeOOH for 24 h at high current density.

The double layer capacitance ( $C_{dl}$ ) measurement was performed to get the correlation of the electrochemically active surface area (ECSA) of the prepared catalysts. The non - faradic capacitive current related to double layer charging was utilized to calculate the  $C_{dl}$ . The S - NiFeOOH exhibited

the  $C_{dl}$  value of  $12.17 \text{ mF cm}^{-2}$ , which was larger than NiFeOOH ( $2.28 \text{ mF cm}^{-2}$ ). The larger value of  $C_{dl}$  indicated the presence of more number of electrochemically available active sites attributed to the S - doping. As a result, the OER

activity was improved due to the greater tendency of water adsorption.

For deep understanding of OER activity, we have determined the number of active sites of the studied catalysts<sup>66</sup>. The reduction peak area integration method was utilized for the evaluation of active sites. The S - NiFeOOH possessed larger number of active sites compared to NiFeOOH. The number of active sites in S - NiFeOOH and NiFeOOH were calculated to be  $6.97 \times 10^{18}$  and  $1.97 \times 10^{18}$ , respectively. The results evidenced the high intrinsic OER activity of S - NiFeOOH in comparison to NiFeOOH. The S - doping in NiFeOOH resulted in the increment of the ECSA, larger number of active sites, lower charge transfer resistance and enhanced electronic conductivity

## 8. Conclusion

In conclusion, we have synthesized S - NiFeOOH on nickel foam by simple solvothermal method for the efficient electrochemical OER activity. The OER activity of S - NiFeOOH was excellent as S - NiFeOOH achieved the current density of  $50 \text{ mA cm}^{-2}$  at merely low overpotential of 200 mV compared to the NiFeOOH. The S - NiFeOOH catalyst showed continuous  $\text{O}_2$  production under chronoamperometric condition for 24 h. The doping of S - atom in NiFeOOH increased the ECSA and number of electrochemical active sites, improved the charge transfer properties and tuned the electronic structure, which resulted in the enhanced OER activity. In summary, our work provides an economic and rational design of heteroatom doped NiFeOOH nanosheets at room temperature with efficient OER activity. Our unique approach can be further extended to develop active metal hydroxide - (oxy) hydroxide catalyst with various metal combination.

### Conflicts of interest

“There are no conflicts to declare.”

### Acknowledgments

Manoj Kumar acknowledges Central Research Facility (CRF) - IIT (Delhi) and IITR - Lab Lucknow for providing the characterization facilities.

### Author Contribution

The synthesis of the catalysts, electrochemical experiments as well as data analysis was performed by Manoj Kumar. Raghvendra Pratap Singh assisted in the data analysis and data curation. The manuscript is written by the contribution of all co - authors. All the authors have given the approval to the final version of manuscript. The conceptualization, editing and reviewing was performed by Raghvendra Pratap Singh

## References

[1] X. Liu, J. Chi, B. Dong and Y. Sun, *ChemElectroChem*, 2019, **6**, 2157–2166.  
 [2] X. Zeng, Y. Bai, S. M. Choi, L. Tong, R. M. Aleisa, Z. Li, X. Liu, R. Yu, N. V. Myung and Y. Yin, *Mater. Today Nano*, 2019, **6**, 100038.  
 [3] Z. N. Zahran, E. A. Mohamed, Y. Tsubonouchi, M. Ishizaki, T. Togashi, M. Kurihara, K. Saito, T. Yui and

M. Yagi, *Energy Environ. Sci.*, 2021, **14**, 5358–5365.  
 [4] A. K. Singh, S. Ji, B. Singh, C. Das, H. Choi, P. W. Menezes and A. Indra, *Mater. Today Chem.*, 2022, **23**, 1–27.  
 [5] B. Singh and A. Indra, *Mater. Today Energy*, 2020, **16**, 100404.  
 [6] L. M. Cao, D. Lu, D. C. Zhong and T. B. Lu, *Coord. Chem. Rev.*, 2020, **407**, 213156.  
 [7] P. W. Menezes, A. Indra, D. González - Flores, N. R. Sahraie, I. Zaharieva, M. Schwarze, P. Strasser, H. Dau and M. Driess, *ACS Catal.*, 2015, **5**, 2017–2027.  
 [8] D. Wang, T. Sheng, J. Chen, H. F. Wang and P. Hu, *Nat. Catal.*, 2018, **1**, 291–299.  
 [9] J. Di, H. Zhu, J. Xia, J. Bao, P. Zhang, S. Z. Yang, H. Li and S. Dai, *Nanoscale*, 2019, **11**, 7239–7246.  
 [10] L. Zhang, W. Cai and N. Bao, *Adv. Mater.*, 2021, **33**, 1–10.  
 [11] W. Ahn, M. G. Park, D. U. Lee, M. H. Seo, G. Jiang, Z. P. Cano, F. M. Hassan and Z. Chen, *Adv. Funct. Mater.*, 2018, **28**, 1–11.  
 [12] D. Zhao, Y. Lu and D. Ma, *Molecules*, DOI: 10.3390/molecules25102304.  
 [13] B. Singh and A. Indra, *Mater. Today Chem.*, 2020, **16**, 100239.  
 [14] K. Fan, H. Zou, Y. Lu, H. Chen, F. Li, J. Liu, L. Sun, L. Tong, M. F. Toney, M. Sui and J. Yu, *ACS Nano*, 2018, **12**, 12369–12379.  
 [15] Y. Tian, S. Wang, E. Velasco, Y. Yang, L. Cao, L. Zhang, X. Li, Y. Lin, Q. Zhang and L. Chen, *iScience*, 2020, **23**, 100756.  
 [16] H. Sun, Y. Zhu, W. Jung, J. Wang, X. Qian and H. Kong, DOI: 10.3390/molecules26185476.  
 [17] T. Wang, H. Chen, Z. Yang, J. Liang, S. Dai, T. Wang, H. Chen, Z. Yang, J. Liang and S. Dai, DOI: 10.1021/jacs.9b12377.  
 [18] J. Suntivich, K. J. May, H. A. Gasteiger, J. B. Goodenough and Y. Shao - Horn, *Science (80 - .)*, 2011, **334**, 1383–1385.  
 [19] Y. Lee, J. Suntivich, K. J. May, E. E. Perry and Y. Shao - Horn, *J. Phys. Chem. Lett.*, 2012, **3**, 399–404.  
 [20] F. Song, L. Bai, A. Moysiadou, S. Lee, C. Hu, L. Liardet and X. Hu, *J. Am. Chem. Soc.*, 2018, **140**, 7748–7759.  
 [21] A. Indra, P. W. Menezes and M. Driess, *ChemSusChem*, 2015, **8**, 776–785.  
 [22] J. Wang, S. J. Kim, J. Liu, Y. Gao, S. Choi, J. Han, H. Shin, S. Jo, J. Kim, F. Ciucci, H. Kim, Q. Li, W. Yang, X. Long, S. Yang, S. P. Cho, K. H. Chae, M. G. Kim, H. Kim and J. Lim, *Nat. Catal.*, 2021, **4**, 212–222.  
 [23] A. Indra, P. W. Menezes, N. R. Sahraie, A. Bergmann, C. Das, M. Tallarida, D. Schmeißer, P. Strasser and M. Driess, *J. Am. Chem. Soc.*, 2014, **136**, 17530–17536.  
 [24] A. Indra, T. Song and U. Paik, *Adv. Mater.*, 2018, **30**, 1–25.  
 [25] A. K. Tareen, G. S. Priyanga, K. Khan, E. Pervaiz, T. Thomas and M. Yang, *ChemSusChem*, 2019, **12**, 3941–3954.  
 [26] F. Lyu, Q. Wang, S. M. Choi and Y. Yin, *Small*, 2019, **15**, 1–17.  
 [27] P. W. Menezes, A. Indra, P. Littlewood, M. Schwarze, C. Göbel, R. Schomäcker and M. Driess, *ChemSusChem*, 2014, **7**, 2202–2211.  
 [28] P. W. Menezes, A. Indra, C. Das, C. Walter, C. Göbel, V. Gutkin, D. Schmeißer and M. Driess, *ACS Catal.*,

- 2017, **7**, 103–109.
- [29] P. W. Menezes, A. Indra, O. Levy, K. Kailasam, V. Gutkin, J. Pfrommer and M. Driess, *Chem. Commun.*, 2015, **51**, 5005–5008.
- [30] P. W. Menezes, A. Indra, A. Bergmann, P. Chernev, C. Walter, H. Dau, P. Strasser and M. Driess, *J. Mater. Chem. A*, 2016, **4**, 10014–10022.
- [31] A. Indra, P. W. Menezes, I. Zaharieva, H. Dau and M. Driess, *J. Mater. Chem. A*, 2020, **8**, 2637–2643.
- [32] J. Huang, J. Chen, T. Yao, J. He, S. Jiang, Z. Sun, Q. Liu, W. Cheng, F. Hu, Y. Jiang, Z. Pan and S. Wei, *Angew. Chemie - Int. Ed.*, 2015, **54**, 8722–8727.
- [33] A. Indra, P. W. Menezes, C. Das, C. Göbel, M. Tallarida, D. Schmeißer and M. Driess, *J. Mater. Chem. A*, 2017, **5**, 5171–5177.
- [34] H. H. Zou, C. Z. Yuan, H. Y. Zou, T. Y. Cheang, S. J. Zhao, U. Y. Qazi, S. L. Zhong, L. Wang and A. W. Xu, *Catal. Sci. Technol.*, 2017, **7**, 1549–1555.
- [35] B. Singh and A. Indra, *Chem. - An Asian J.*, 2020, **15**, 607–623.
- [36] Y. Zuo, D. Rao, S. Ma, T. Li, Y. H. Tsang, S. Kment and Y. Chai, *ACS Nano*, 2019, **13**, 11469–11476.
- [37] Y. Wang, D. Yan, S. El Hankari, Y. Zou and S. Wang, *Adv. Sci.*, DOI: 10.1002/advs.201800064.
- [38] B. Singh, A. Yadav and A. Indra, *J. Mater. Chem. A*, 2022, **10**, 3843–3868.
- [39] B. Singh, A. K. Patel and A. Indra, *Mater. Today Chem.*, 2022, **25**, 1–24.
- [40] J. Hu, S. Li, J. Chu, S. Niu, J. Wang, Y. Du, Z. Li, X. Han and P. Xu, *ACS Catal.*, 2019, 10705–10711.
- [41] M. Asnavandi, Y. Yin, Y. Li, C. Sun and C. Zhao, *ACS Energy Lett.*, 2018, **3**, 1515–1520.
- [42] Y. Wu, H. Wang, S. Ji, X. Tian, G. Li, X. Wang and R. Wang, *Appl. Surf. Sci.*, 2021, **564**, 150440.
- [43] J. J. Zhang, W. W. Bao, M. Y. Li, C. M. Yang and N. N. Zhang, *Chem. Commun.*, 2020, **56**, 14713–14716.
- [44] P. Ma, S. Luo, Y. Luo, X. Huang, M. Yang, Z. Zhao, F. Yuan, M. Chen and J. Ma, *J. Colloid Interface Sci.*, 2020, **574**, 241–250.
- [45] H. S. Chavan, C. H. Lee, A. I. Inamdar, J. Han, S. Park, S. Cho, N. K. Shreshta, S. U. Lee, B. Hou, H. Im and H. Kim, *ACS Catal.*, 2022, **12**, 3821–3831.
- [46] M. X. Jin, Y. L. Pu, Z. J. Wang, Z. Zhang, L. Zhang, A. J. Wang and J. J. Feng, *ACS Appl. Energy Mater.*, 2019, **2**, 4188–4194.
- [47] J. Li, J. Song, B. Y. Huang, G. Liang, W. Liang, G. Huang, Y. Qi Jin, H. Zhang, F. Xie, J. Chen, N. Wang, Y. Jin, X. B. Li and H. Meng, *J. Catal.*, 2020, **389**, 375–381.
- [48] R. Guo, Y. He, T. Yu, P. Cheng, J. You, H. Lin, C. Te Chen, T. Chan, X. Liu and Z. Hu, *Chem. Eng. J.*, 2021, **420**, 127587.
- [49] X. Cui, Z. Chen, Z. Wang, M. Chen, X. Guo and Z. Zhao, *ACS Appl. Energy Mater.*, 2018, **1**, 5822–5829.
- [50] J. Wang, T. Liao, Z. Wei, J. Sun, J. Guo and Z. Sun, *Small Methods*, 2021, **5**, 1–27.
- [51] M. Kumar and R. P. Singh, 1–16.
- [52] Y. F. Yuan, X. H. Xia, J. B. Wu, J. L. Yang, Y. B. Chen and S. Y. Guo, *Electrochim. Acta*, 2011, **56**, 2627–2632.
- [53] P. Prieto, V. Nistor, K. Nouneh, M. Oyama, M. Abd - Lefdil and R. Díaz, *Appl. Surf. Sci.*, 2012, **258**, 8807–8813.
- [54] J. Ran, J. Yu and M. Jaroniec, *Green Chem.*, 2011, **13**, 2708–2713.
- [55] J. Baltrusaitis, D. M. Cwiertny and V. H. Grassian, *Phys. Chem. Chem. Phys.*, 2007, **9**, 5542–5554.
- [56] T. Yamashita and P. Hayes, *Appl. Surf. Sci.*, 2008, **254**, 2441–2449.
- [57] C. Long, L. Jiang, T. Wei, J. Yan and Z. Fan, *J. Mater. Chem. A*, 2014, **2**, 16678–16686.
- [58] M. Wahlqvist and A. Shchukarev, *J. Electron Spectros. Relat. Phenomena*, 2007, **156–158**, 310–314.
- [59] B. Singh, O. Prakash, P. Maiti, P. W. Menezes and A. Indra, *Chem. Commun.*, 2020, **56**, 15036–15039.
- [60] B. Singh, O. Prakash, P. Maiti and A. Indra, *ACS Appl. Nano Mater.*, 2020, **3**, 6693–6701.
- [61] B. Singh and A. Indra, *Dalt. Trans.*, 2021, **50**, 2359–2363.
- [62] H. Wang, H. S. Casalongue, Y. Liang and H. Dai, *J. Am. Chem. Soc.*, 2010, **132**, 7472–7477.
- [63] H. Su, X. Zhao, W. Cheng, H. Zhang, Y. Li, W. Zhou, M. Liu and Q. Liu, *ACS Energy Lett.*, 2019, **4**, 1816–1822.